Optical trapping for undergraduates

D. C. Appleyard
Department of Biological Engineering, Massachusetts Institute of Technology,
Cambridge, Massachusetts 02139

K. Y. Vandermeulen
Department of Materials Science and Engineering, Massachusetts Institute of Technology,
Cambridge, Massachusetts 02139

H. Lee
Department of Mechanical Engineering, Massachusetts Institute of Technology,
Cambridge, Massachusetts 02139

M. J. Lang[a)]
Department of Biological Engineering and Department of Mechanical Engineering,
Massachusetts Institute of Technology, Cambridge, Massachusetts 02139

The detailed design of a robust and inexpensive optical trap system is presented. The system features high-sensitivity back focal plane position detection, mechanically controlled specimen stage movement, and fluorescence imaging to provide broad experimental applications. Three educational experimental modules are described to cover basic concepts in optical trapping and biophysics at a level appropriate for undergraduate students. © *2007 American Association of Physics Teachers.*
[DOI: 10.1119/1.2366734]

I. INTRODUCTION

The discovery and demonstration of applied radiation pressure by Ashkin established the foundation for research using optical force probes, such as optical tweezers and optical traps.[1] The application of these tools to biological problems has enabled a myriad of new experiments focusing on single molecule biophysical systems, including studies of DNA, molecular motors such as kinesin and myosin, and cell level studies.[2–6] Such rapid proliferation of experiments utilizing optical traps indicates the integral position that this technology has found in the research laboratory. It also points to the increasing importance of developing instruments suitable for educational use. We have developed such a system, which is simple, inexpensive, and robust. It is suitable for a wide range of experiments and teaching applications. Our focus will be on applications in biophysics and biomechanics for an advanced undergraduate laboratory.

Our system builds and expands on previous work on educational instruments.[7–10] The present optical trap can perform a wider range of experiments through the integration of a quadrant photodiode for back focal plane position detection, a near infrared wavelength trapping laser, and a 532 nm laser diode with optics for incorporating fluorescence imaging.[11] The fluorescence capabilities are sufficient to image individual rhodamine labeled microtubules and the quadrant photodiode position detection system can resolve steps of nearly 6 nm. In addition, the mechanical automation of specimen stage motion enables force probe calibration with the Stokes drag method. This combined setup, which is arranged around a custom inverted microscope design, has a compact footprint for improved portability and for use in laboratories where there are space constraints. The entire setup can be built for under $15 000 using primarily off the shelf optomechanical elements.

To complement this straightforward design, we discuss three educational modules based on classical experiments that highlight general concepts of optical trapping, basic tenants of biophysical measurements, and the state of the art capabilities of this instrument. The first lab module covers the basics of trap characterization and calibration. Two additional modules explore experiments on single molecule biomechanics through the measurement of *E. coli* rotation in a tethered bacterium assay and by observing DNA stretching in a tethered bead assay.

II. INSTRUMENT DESIGN

The following description highlights the major features of the instrument design. Additional information on construction and assembly is available in the supplementary materials, including drawings of machined parts, circuit layouts, and tips on alignment.[12]

Unlike the majority of optical trapping setups that are built around commercial microscope platforms, our instrument is based on a handmade microscope core. A detailed diagram of the optical layout is presented in Fig. 1 and images of the assembled system are available in the supplementary information.[12] All system components are mounted on a 2 × 2 ft² breadboard to save space, increase portability, and promote stability by minimizing optical path distances.[11]

A. Trapping laser path

The heart of an optical trap is the trapping laser for which we use a near infrared fiber-coupled source at 975 nm (975, Avanex, 3CN00283AC). This choice affords sufficient power (up to 150 mW) to form a stiff trap and includes a Bragg grating to stabilize the lasing wavelength and prevent laser mode hopping. Visible lasers used in other instruments offer advantages in alignment; however, this near infrared wavelength laser is low cost, optimal for biological applications, does not require an optical isolator, and leaves the visible spectrum open for fluorescence microscopy.[11]

The laser is collimated by adjusting the distance between a cage plate (Thorlabs CP01) machined to hold the laser fiber
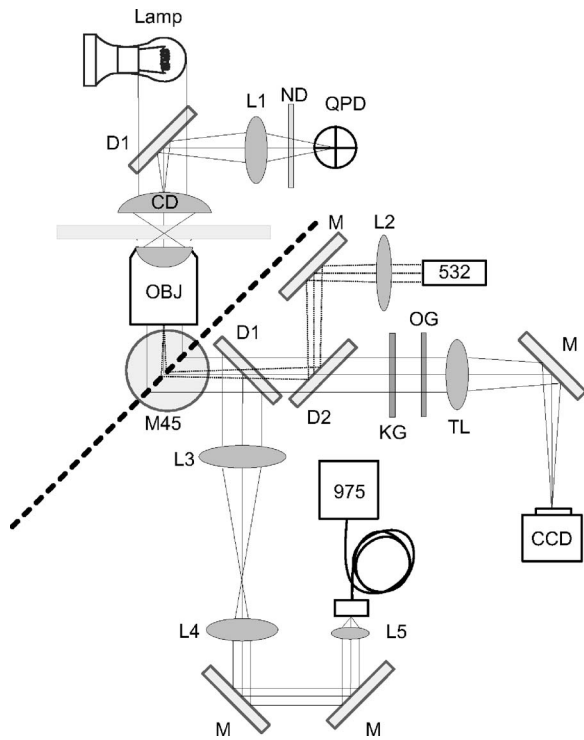
Fig. 1. Optical layout of the tweezer setup. The dashed line at 45° indicates separation between components placed horizontally on the breadboard (lower right) and those raised vertically (upper left) as part of the inverted microscope. ND: neutral density filter, QPD: quadrant photodiode, OBJ: objective, CD: condenser, 532: 532 nm fluorescence excitation laser, 975: 975 nm near infrared trapping laser, M: mirror, M45: mirror oriented at 45° to the optical breadboard connecting horizontal components (lasers) and vertical components (objective and detector), L1: 35 mm lens, L2: 300 mm lens, L3: 100 mm lens, L4: 60 mm lens, L5: 11 mm lens, D1: IR reflective dichroic, D2: 532 reflective dichroic, KG: visible pass filter, OG: long pass filter, TL: tube lens, and CCD: charge-coupled device firewire camera.

and a mounted 11 mm focal length aspherical lens (L5, Thorlabs C220TM-B).[12] Alternatively, machining of the cage plate can be avoided by terminating the fiber with a ferrule connector and using a FC mount (Thorlabs SM1FCA). The collimated beam is 1.6 mm in diameter and is further expanded to 2.7 mm with a telescope consisting of two lenses with focal lengths of 100 and 60 mm (L3 and L4, Thorlabs AC254-100-B and AC254-60-B). An *XY* mount (Thorlabs LM1XY) for the 60 mm lens permits mechanical steering of the trap in the sample plane. Two silver mirrors (M, Thorlabs PF10-03-P01) facilitate alignment of the beam parallel to the breadboard. The separation of visible light and near infrared paths occurs at the dichroic (D1, Thorlabs FM01) after the telescope. A mirror oriented at 45° to the breadboard (M45, Thorlabs PF10-03-P01) reflects the light path vertically toward the objective. The objective focuses the beam to create the trap, and the back-scattered and transmitted light collected by the condenser is directed into the detection branch.

B. Inverted microscope

As mentioned, the trapping apparatus is constructed around a handmade inverted microscope core. We choose the inverted microscope design for its stability and ease of multiple beam incorporation, and as an arrangement where gravity drives sample beads to the coverglass surface. A solid mechanical layout promotes stability of the optics and

sample, with a 1.5 in. vibration damped post (Melles Griot 07 DUP 12) forming the backbone of the inverted design. Two vertically oriented translation mounts (Thorlabs MT1) are attached to the post, providing mounting points for custom L-shaped adapter brackets that hold the objective and condenser.[12]

The objective used, a 100×1.25 NA (OBJ, Nikon), has a back aperture of 5 mm, larger than the trapping beam diameter of 2.7 mm. Trapping theory dictates that overfilling the back aperture provides the stiffest trap possible, taking full advantage of the numerical aperture of the objective.[13] A few considerations motivate our non-stiffness-optimized design. Due to the numerical aperture (NA) of the condenser and the optics within the detection branch, the best sensitivity to bead position is obtained at a 100:600 expansion. Our choice of lenses for the telescope balanced focal length versus space available on the breadboard and aberrations experienced with short focal length lenses. The $1.67 \times$ expansion provides a trap stiffness that is sufficient for the experimental applications of interest.

An air spaced infinity condenser, numerical aperture 0.9, $40 \times$ (CD, Nikon 92381), delivers bright field illumination and collects the scattered trap beam for position detection. This choice of condenser avoids the use of oil and permits ease of loading samples. A white light source (Maglite AA Mini-Maglite) is mounted above the condenser and supplies ~2900 candela of illumination for bright-field imaging.

C. Detection branch

The position detection branch is mounted above the condenser using a machined plate (Thorlabs CP01).[12] A cage cube (Thorlabs C4 W) holds a dichroic mirror (D1, Thorlabs FM01) that reflects the 975 nm beam toward the detector while passing the white light illumination. A 35 mm focal length lens (L1, Thorlabs LB1811) forms an image conjugate to the condenser back focal plane on a quadrant photo diode (UDT Spot 9DMI) set in an *X-Y* translation mount (Thorlabs HPT1). A quadrant photodiode was used as the most cost effective option, although more sensitive and faster position sensitive devices are available. A neutral density filter (ND, Thorlabs NE20B) attenuates light intensity to avoid saturating the detector.

A handmade detection circuit is used to provide a -10 to 10 V signal. The design follows those in the literature and is available in the supplementary materials.[12,14] The circuitry is designed to have a bandwidth of ~20 kHz, approximately an order of magnitude greater than the expected rolloff frequency characteristic of trapped bead motion.[11]

D. Other subsystems

For white light imaging of samples, the eyepiece is deliberately omitted to reduce cost and enhance the safety of the instrument. Instead, imaging is accomplished using a 640×480 CCD firewire camera (CCD, ImagingSource DMK 21F04), which is placed at an image plane formed by a 200 mm focal length tube lens (TL, Nikon 93020). Filters eliminate either the 975 nm beam (KG, Schott KG5) or the fluorescence excitation wavelength (532 nm) (OG, Schott OG570). These filters can be removed for alignment or demonstration purposes, although care must be used to prevent damage to the CCD camera.

A three-axis stage (Newport 562 ULTRAlign) affords a stable and smooth translation mount for the sample. It is elevated above the breadboard using a 1.5 in. post (Thorlabs P3). Two machined bars with slide clips suspend the slide over the objective.[12] The integration of two picomotors (New Focus 8301) to replace the micrometers permits automated X and Y stage position control and movement with a step increment of ~30 nm, albeit with some hysteresis. This control facilitates the calibration of the position detection, permits Stokes drag calibrations, and extends the versatility of the instrument.

For fluorescence excitation, a low cost 3 mW laser (532, World Star Tech DPGL-03S-TTL) at 532 nm offers ample power for fluorescence imaging. A dichroic mirror (D2, Chroma Z532RDC) integrates the excitation laser into the optical path. A long pass filter placed before the CCD camera (CVI CG-OG-570-1.00-2.0) eliminates any remaining excitation illumination. A 300 mm lens (L2, Thorlabs LB1779) focuses the 532 nm excitation laser at the back focal plane of the objective to make the region of sample illumination larger.

A high speed computer-based data acquisition system is used to log data and automate stage movement (National Instruments PCI-6070E). Labview software provides integrated control and data acquisition for the system. Examples of acquisition and control software are available in the supplementary materials.[12] Data analysis was done using Matlab.

E. Safety

Appropriate safety measures must be taken with Class IIIb trap and excitation lasers, one of which is not visible to the naked eye in use in an undergraduate environment. An enclosure was built to encompass all of the horizontal optical components, blocking any stray reflections and limiting access to the beam path. The enclosure has the added advantage of blocking room light from disrupting the CCD image quality. We recommend enclosing the entire instrument with laser interlocks for additional safety. It is imperative to discuss laser safety with students prior to laboratory experimentation to reduce the possibility of injury.

III. EXPERIMENT: CALIBRATION

Optical trap calibration procedures are central for students' foundation in the physical properties of the microscopic environment. Here they are exposed to units of energy in k_BT, forces in piconewtons, and distances in nanometers. Three calibration procedures, Stokes drag, equipartition, and power spectrum, provide the basis of quantitative measurements using an optical trap and give an essential exposure to methods used in high end instrumentation. Taking these calibration measurements permits students to learn techniques for data acquisition, curve fitting, and analysis while providing essential skills for the other modules.

A. Calibration: Theory

Calibration can be separated into two parts. First, calibration of the detector is required to determine the relation between the voltage signal produced by the detector and the position of the bead with respect to the center of the trap x. The trap behaves as a linear spring, and thus force is calculated by measuring the displacement out of the trap center

and the spring constant k, the second value required. These two calibrations provide the parameters to calculate the force exerted by the trap by the relation $F=kx$. Position and stiffness values are calibrated for both lateral axes of stage motion, because the position response and trap stiffness will vary due to the laser beam profile and polarization.

1. Position calibration

In our design three methods are available for determining the position calibration, one based on video and two using the quadrant photodiode. The video is slower and requires significant postprocessing of data. Though this instrument is capable of video position detection, it is unused because the quadrant photodiode has a faster response time. The video method relies on extracting the pixel position of an object from different frames in a sequence of motion. The difference in pixel positions is calculated and a pixel to nanometer conversion is applied to yield quantitative movement. This conversion factor can be determined by using a ruled microscope slide or precisely known movements of an object.

We use two position calibration methods involving the quadrant photodiode. Rather than relying on video, these methods of calibration report the location of a trapped bead by converting the back focal plane image of the laser scatter to an X and Y voltage signal that is converted to nanometers of displacement. The first quadrant photodiode technique involves scanning a sample target bead immobilized on the surface through a grid of known displacements with automated stage movement and mapping the voltage response of the quadrant photodiode.[15] This method is straightforward and quick. It requires accurate, reproducible, and automated movement of the bead relative to the trap, which can be a costly part of the design and can be achieved using piezo stages.

The second quadrant photodiode technique is outlined in Refs. 16 and 17. It focuses on extracting the voltage to nanometer conversion of the quadrant photodiode directly from the power spectrum of a trapped bead. In an optical trap the power spectral density of a trapped bead has a Lorentzian profile described by[13,16,18]

$$S_{VV}(f) = \rho^2 \frac{k_BT}{\pi^2 \beta (f_0^2 + f^2)}, \tag{1}$$

where $S_{VV}(f)$ is the uncalibrated power spectrum with units of V^2/Hz, f is the frequency, k_B is Boltzmann's constant, β is the drag coefficient equal to $6\pi\eta r$, where η is the viscosity of the fluid medium, r is the radius of the bead, T is the absolute temperature, ρ is the linear voltage to displacement calibration factor, and f_0 is the corner frequency.

The multiplication of the power spectrum by f^2 results in a constant value of $S_{VV}(f)\ f^2$ at high frequencies where $f \gg f_0$.[16] If we use this constant value and rearrange the terms, we obtain

$$\rho = \left(\frac{S_{VV}(f \gg f_0)f^2 \pi^2 \beta}{k_BT} \right)^{1/2}. \tag{2}$$

The position calibration value ρ has units of voltage/displacement. This method is very useful for the instrument if controlled stage motion is absent.

2. Trap stiffness calibrations

With position calibration completed, the stiffness of the trap can be evaluated in several ways. The Stokes drag calibration method measures the displacement of a trapped bead out of the center of the trap caused by balancing the external drag force applied by the fluid flow with the restoring force of the trap. The measurement is made by translating the sample chamber at a controlled velocity and inducing a well defined laminar drag flow about the trapped bead. For a spherical bead the drag force is $6\pi\eta r v$, where v is the velocity of the fluid. The stiffness of the trap k can be equated to this force for a displacement x from the center of the trap as

$$kx = 6\pi\eta r v. \tag{3}$$

If the bead is near the coverglass surface, it will experience boundary layer effects changing the viscous drag coefficient. These can be accounted for using Faxen's law correction.[14]

The second calibration method is based on the equipartition theorem, which states that each degree of freedom in a harmonic potential has $k_B T/2$ of energy. This relation can be used to relate the measurement of the instantaneous displacement of a trapped particle to the available thermal energy of a system defined as

$$\frac{1}{2}k_B T = \frac{1}{2}k\langle(x - x_{\text{mean}})^2\rangle. \tag{4}$$

The equipartition method does not rely on specific information of the medium, viscous drag, or particle size and shape; however, this method requires calibration of the position detection.

The final method of calibration also relies on the thermal motion of a trapped bead and the Lorentzian profile of the power spectrum given in Eq. (1). The rolloff or corner frequency of the power spectrum provides the trap stiffness as

$$k = f_0 2\pi\beta. \tag{5}$$

This method is independent of the detector voltage to displacement calibration, which is a significant advantage in an instrument lacking integrated stage motion or some other means to provide position calibration. Again a fast (>10 kHz) acquisition rate is required, necessitating care in the choice of detector and detector circuitry.[18]

B. Calibration: Materials and methods

The goal of this section is to acquire three data sets. First, a voltage trace of the thermal motion of a trapped bead is gathered. These data will be used in the power spectrum and equipartition methods to calculate a position calibration based on the fit of the power spectral density to the Lorentzian as described in Eq. (1). Secondly, a voltage versus stage velocity measurement is taken to allow Stokes drag calculations. Finally, a quadrant photodiode voltage to position calibration generated by stepping a bead stuck on the slide through the trap is completed. To fully characterize the instrument, these measurements are repeated to cover a range of laser intensities. Because the stiffness should track linearly with laser power, the instrument can be calibrated by sweeping the available range of laser power output.

A slide with beads both stuck to the surface and free in solution is optimal for performing calibrations. A flow cell is created by placing two pieces of double sided sticky tape
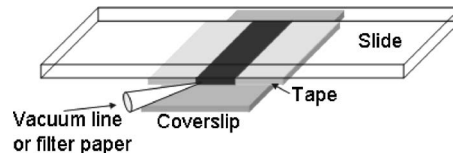

Fig. 2. Diagram of a flow channel (black) constructed from a standard microscope slide, two pieces of double sided sticky tape (light gray), and a coverslip (dark gray). The channel is about 3–4 mm wide. A vacuum line can be used to flush the sample chamber.

across the center of a standard microscope slide to form a 3–4 mm wide channel. A coverslip is placed over the top of the tape, perpendicular to the microscope slide, and firmly sealed, forming a channel with a volume around 15 μL as shown in Fig. 2. The exchange of channel contents is done by depositing the new solution on the coverslip on one side of the channel and then drawing the solution through from the other side. A vacuum setup with a pipette tip at one end can provide suction to draw the fluid. Alternatively, using the tip of a wedge of filter paper provides suction by capillary action. Maintaining a flow rate below $\sim$100 μL/min is reasonable for the applications discussed here. To affix beads on the surface of a slide a 1 M NaCl solution containing beads at a 1:1000 dilution of 10 wt% stock beads (1 μm silica, Bangs SS03N/4669) is loaded into the channel and allowed to incubate for 1 h. The channel is then flushed with 300 μL of water using the vacuum to displace the salt solution. Suspended beads, a 1:50 000 dilution of the same 10 wt% beads in water, is then loaded. The channel is finally sealed with nail polish or vacuum grease to prevent evaporation.

The slide is loaded on the sample stage with a single drop of immersion oil placed between the objective and coverglass. The air spaced condenser is lowered to a predetermined position where it collimates the exiting laser beam. To facilitate focusing on the surface, students can first position the slide so that the center of the lens is near the tape-water boundary. Translating the slide laterally will help to find the tape/flow chamber boundary; focusing the slide along the optical axis can then be used to locate the coverglass surface.

The next step is to ready the detector by zeroing the signal. With a suspended bead trapped, the quadrant photodiode is moved in the mount to zero the X and Y signals. A sample trace of the detector voltage in X and Y is collected (Fig. 3)
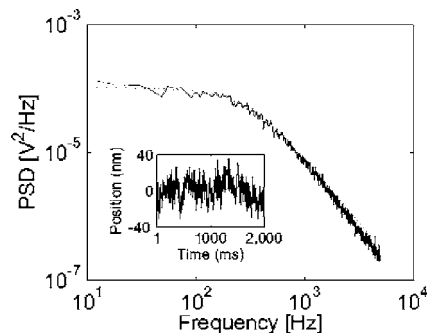

Fig. 3. Power spectral density of a bead in the trap fitted to a Lorentzian curve (dashed line) where the rolloff frequency can be extracted to calculate stiffness. This measurement at 30 mW yielded a stiffness of 0.0246 pN/nm from the rolloff. Inset: Position versus time data used to calculate the equipartition stiffness from Eq. (4). For this measurement at 30 mW the equipartition stiffness was 0.0242 pN/nm.
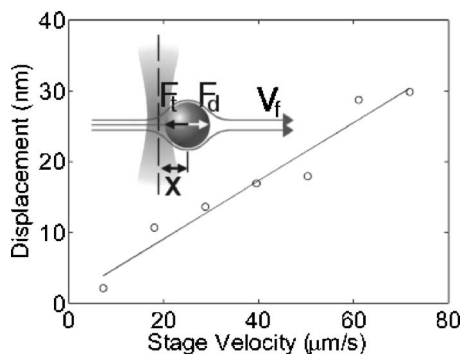
Fig. 4. Stokes drag method for determining trap stiffness. Open circles: The displacement x of the 1 μm bead out of the trap was taken for various stage velocities, which is equivalent to the fluid velocity V_f. Solid line: Linear fit of the displacement to the stage velocity; the slope is k/β as in Eq. (3). The calculated stiffness at 30 mW was 0.0322 pN/nm. Inset: Cartoon of Stokes flow measurement. F_d is the drag force caused by flow V_f, F_t is the restoring force from the trap.

Table I. Measured trap stiffness for the Y axis using the three methods of calibration.

	Stiffness (pN/nm)			
	30 mW	60 mW	90 mW	120 mW
Lorentzian	0.024	0.044	0.057	0.066
Equipartition[a]	0.023	0.045	0.061	0.068
Stokes Drag[a]	0.033	0.057	0.067	0.106
Equipartition[b]	0.010	0.019	0.038	0.052
Stokes Drag[b]	0.020	0.036	0.054	0.090

[a]Calculations using the position calibration from the Lorentzian, Eq. (1).
[b]Calculations using the position calibration from a scanned stuck bead.

the position detection uses the same laser as the trap, the position to voltage calibration must be repeated at each new power level.

C. Calibration: Experimental results

Our goal is to expose students to the capabilities of a high end instrument while keeping costs down and maintaining ease of use. Because some points of our design sacrifice optimal trapping and detection, perfect agreement between the calibration methods will not occur. One example is the use of an air spaced condenser with smaller diameter optics on the detection branch that restrict the aperture of the detection beam. Additionally, high end research instruments use separate trapping and detector beams combined with automated optics to facilitate position calibration using a bead in solution rather than one stuck to the coverslip.[19] We have observed that the in-solution bead calibration values diverge from the stuck bead calibration values as the numerical aperture of the condenser is restricted. This difference is one reason position calibration values reported using varying methods differ and may either directly or indirectly affect the agreement between the stiffness calibrations. Finally, the picomotors used to do a stuck bead position calibration exhibit some random step size distribution and demonstrated off axis motion.

The roll off and equipartition methods show the closest agreement for stiffness measurements (see Table I) when the power spectrum method of position calibration is used. This agreement is not surprising because these techniques use the same data set and are inherently linked methods.

The largest inconsistency in stiffness calibration was with the Stokes method. At laser powers below 100 mW, the values were within a factor of 2 of those obtained by equipartition or the power spectrum. At laser powers above 100 mW the deviation reached a factor of 2. Here the variation can likely be attributed to the inconsistent picomotor speed as well as changes in focus and the slide environment during motion. Another attribute that contributed to inconsistency was the difficulty in controlling the exact height of the bead above the surface. The height directly determines the boundary effects caused by surface proximity and could lead to variations of the calibration methods.

The detection circuitry provides sufficient bandwidth for the trap stiffnesses encountered with our design. However, if the trap stiffness increases significantly, the circuitry will skew data on rolloff measurements because the electronic filter will impose and artificially lower the rolloff frequency.

at 100 kHz. The fastest acquisition speed is used so that ample bandwidth is available for the Lorentzian and equipartition measurements.

To do the Stokes drag measurement a bead is held in the trap while the stage is translated at a set velocity to produce a uniform drag flow around the bead (Fig. 4, inset). The detector voltage is captured simultaneously to measure the displacement of the bead caused by the drag force. A series of stage velocities is used to produce a range of bead displacements (Fig. 4).

Finally, a position calibration must be acquired. This process involves scanning a stuck bead through the focused trap beam in the X-Y plane. A stuck bead is placed in the center of the trap, where the X and Y voltage is zero. This zero point, labeled A in Fig. 5, should reside between the maximum and minimum voltage measured during the bead scan. Acquiring the calibration for one axis involves incrementally moving the stage in uniform steps of a defined displacement while recording the detector voltage. The bead is recentered and the other axis is scanned. To fully characterize the detector region a scan of 3 μm is sufficient and a step size of 30 nm provides adequate resolution. The voltage to position data can be fit to a line or a third-order polynomial to complete the calibration (Fig. 5).

Full characterization of the detector response involves repeating the calibrations at a range of laser powers. Because
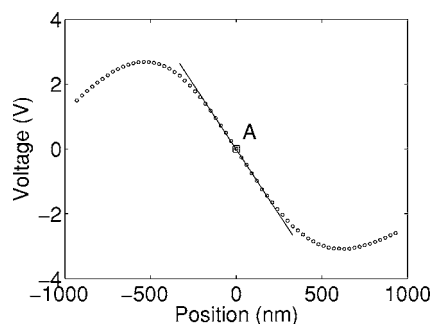

Fig. 5. Scan of a 1 μm stuck bead used to determine the position calibration for the detector. Circles: Acquired data. Solid line: Linear fit for calibration coefficient of $\sim$128.5 nm/V. Label A indicates a zero point where the bead is in the center of the detector.

We found the position calibrations to be consistent above 70 mW and recommend the power spectrum method for lower powers. Because of the lack of dependence on position calibration, we used the stiffness derived from the power spectrum for a majority of the experiments. We encourage researchers and students alike to characterize their own instrument to evaluate which method works best.

IV. EXPERIMENT: ROTATING *E. COLI*

The low force regime at which optical traps work make them optimal for investigating the mechanical output of biological molecular motors.[4,20] A supply of flagellar motors that are easy to work with can be found by using the bacterium *E. coli*. The bacterial populations are easy to culture and simple to visualize with a light microscope, making them optimal for this laboratory environment.

The tethered bacterium or rotating bacterial cell assay uses torque from the flagellar motor to rotate the body of the cell. This robust assay has been used to study chemotaxis and the biophysics of the flagellar motor.[21,22] Additionally, the visual nature of the experiment quickly captures the students' attention. For students this assay provides access to molecular motors, highlights scientific estimation, uses the time and frequency domain representation, and exposes them to doing collaborative studies. Probing flagellar motion can seed discussion of bacterial propulsion including random walks as well as life at low Reynolds number.[23]

Two characteristics that can be quantified individually with *E. coli* using the optical trap are the rotation frequency and stall torque of the flagellar motor.[22] In this module a weak trap can monitor rotation and a strong trap can be used to halt rotation. The ease with which measurements can be collected supports the compilation of population data and the opportunity to explore the heterogeneity in a sample.

A. *E. coli*: Materials and methods

To easily measure rotation parameters a specific strain of *E. coli* that can quickly attach to the coverslip is required. The KAF95 strain is nonpathogenic, exhibits only clockwise rotation, and has sticky flagellum that can attach to glass.[24] Samples of KAF95 are available to institutions uponc request. A small sample of *E. coli* can be grown in culture and then either frozen for future use as an inoculation or used directly in the experiment. To grow a culture, 10 mL of a solution containing 10 mg/mL Bacto-Tryptone (Becton, Dickinson and Company), 5 mg/ml NaCl (Sigma), and 100 μg/mL ampicilin (Sigma) in water is inoculated with a 5–10 μL aliquot of frozen KAF95. This solution is incubated in a water bath at 37 °C for 24–36 h. We suggest that instructors culture the *E. coli* prior to the class; the construction of the *E. coli* slides is simple and can be accomplished by students if facilities are available for wetlab work using biological material. To make the slides, a 15 μL aliquot of the grown culture is loaded into a flow chamber (assembled as described previously) and allowed to incubate for ~5 min to permit bacterial attachment to the coverglass surface. The flow chamber is then flushed with 300 μL of motility buffer (10 mM potassium phosphate, 0.1 mM EDTA, pH 7.4) using vacuum suction to remove unattached bacteria. A 10% bleach solution should be made available for cleanup of the biological samples. Those unfamiliar with the basics of cell
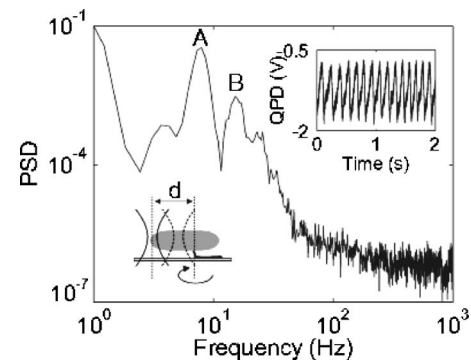

Fig. 6. Power spectral density of the *Y* axis voltage from the quadrant photodiode for a spinning *E. coli* showing a peak near 7 Hz, A, and a harmonic at 14 Hz, B. Inset: Raw *Y* axis quadrant photodiode voltage used to generate a position sensitive device, reflecting a 7 Hz rotation speed. Cartoon: Assay geometry depicting trap position for optimized stalling and monitoring (solid line) and a trap position that is not optimal for stall and would give 2× actual rotation speed (dashed line). The distance between the trap center and point of rotation *d* is indicated.

culture are directed to Ref. 25 for an introduction to these techniques.

The first measurement uses a very weak trap to detect rotation as the bacterium occludes the beam. The trap is set to a laser power just above the lasing threshold (~7 mW) so trap forces will not interfere with rotation. The focus of the optical trap is placed at the edge of the zone through which the rotating bacterium sweeps. The quadrant photodiode voltage signal is collected for both the *X* and *Y* axes (Fig. 6, inset). A power spectral density of a trace of the voltage signal will show a peak identifying the rotation frequency (Fig. 6, label A).

A second measurement seeks the minimum laser power required to stall rotation of the flagellar motor. The laser power is increased to approximately 120 mW (forming a relatively stiff ~0.08 pN/nm trap) and a bacterium is moved into the trap where the tip of the bacteria is trapped in three dimensions and rotation is halted. The laser power is reduced until the bacterium escapes the trap and begins rotating. The approximate trap stiffness at the final power is estimated from a linear fit of previous power calibrations (Sec. III). A calculation of the stall force *F* requires an assumption of the displacement *x* out of the center of the trap. The value of *x* can be estimated by a knowledge of the trap potential or by experimental observation of the maximum displacement at which a bead or bacterium exposed to Stokes flow falls out of the trap. We found an estimate of 100 nm to be reasonable for the displacement in our setup.

The stall torque τ generated by the flagellar motor can then be determined by treating the trap as a point force acting perpendicular to the direction of rotation on the outer tip of the *E. coli* as $\tau = Fd$. This determination requires a measurement of the distance *d* between the rotation point and the tip of the bacteria on which the trap acts. This lever arm length is typically between 1 and 3 μm and can be obtained by visual inspection of images with a calibrated field of view. A simple comparison to the size of a bead offers a quick value. As a general idea of the population characteristics, a majority of the bacteria were between 2 and 3 μm in length. The measurements and estimations used in this procedure provide good discussion points and experience with error estimation,
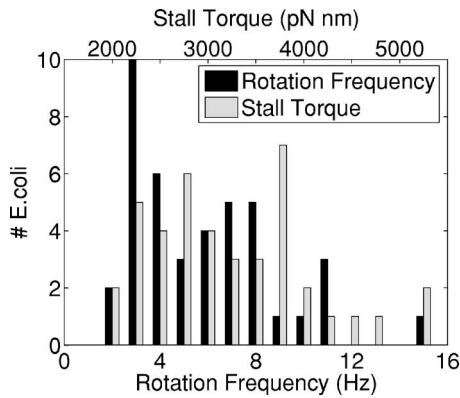
Fig. 7. Population distribution of rotation frequency (bottom abscissa) and stall torque (top abscissa) for a sample of 41 bacteria. The population had an average rotation speed of 5.8 Hz and an average stall torque of 3200 pN nm.

and the results provide a reasonable final value of the stall torque.

B. *E. coli:* Experimental results

A student using the optical trap to measure both rotational speed and stall torque can evaluate about ten individual *E. coli* in an hour. Aggregating data from multiple students can provide a good examination of population characteristics. Representative population distributions of both rotation speed and torque are displayed in Fig. 7.

Despite multiple "back of the envelope" assumptions, the spin rate and estimated torque are within range of previously reported values. The fundamental rotation frequency was easy to extract from both the power spectrum (Fig. 6) and from the raw voltage versus time trace (Fig. 6, inset). The average rotation speed in our sample population was 5.8 Hz, which is within the 2 to 9 Hz rotation speed span noted by Silverman.[26] In some cases the position of the trap relative to the rotating point provided a detector response from both ends of the bacteria, giving a fundamental frequency twice that of the actual (Fig. 6, inset). Often this situation can be diagnosed from the raw voltage signal because each end of the bacteria deflects the trap differently. Stall torque values were estimated using the calculated stiffness for a 1 μm bead, a 100 nm displacement, and the comparison to bead diameter method for determining the lever arm length. We measured an average torque of 3200 pN nm, on the order of the reported value of 4000 pN nm.[22]

V. EXPERIMENT: DNA TETHER EXTENSION

The tethered bead assay is probably the most versatile geometry in optical trapping based single molecule biophysics experiments. This geometry has been widely used with single molecules such as DNA, kinesin, RNA polymerase, and Myosin.[3,4,27,28] The classical experiment underlying the tethered bead assay is the DNA tether stretching measurement. This measurement introduces parameters such as contour length, persistence length, and effective spring constant scaling laws for entropic and enthalpic regions of stretching curves. Here we discuss a module where we stretch a DNA tether between the coverglass surface and a bead. This experiment may be approached on several different levels providing both wet lab experience in preparing the samples and physical insight into the mechanical properties of DNA.

Analysis can include fitting DNA stretching curves with the wormlike chain or more advanced polymer stretching models.[29,30]

A. DNA tether stretching: Background theory

The wormlike chain model has two main parameters, the contour length ℓ_c and the persistence length ℓ_p,[29] and has been used to describe the elastic behavior of DNA.[29] The contour length refers to the end-to-end length of the polymer backbone under no tension, and the persistence length is the length of a segment at which there is no longer a correlation between the direction of the beginning and end of the segment. The persistence length ℓ_p can be defined as

$$\ell_p = \frac{YI}{k_B T}, \tag{6}$$

where Y is the Young's modulus of the material and I reflects the moment of inertia of the cross-section. We use the following interpolation of the wormlike chain model[29]

$$F = \frac{k_B T}{\ell_p}\left[\frac{1}{4}\left(1 - \frac{x}{\ell_c}\right)^{-2} - \frac{1}{4} + \frac{x}{\ell_c}\right], \tag{7}$$

where F is the applied force and x is the end-to-end extension distance of the DNA tether. This interpolation fits the data well for $\ell_p \ll \ell_c$ and $F < 5$ pN.[30] Modifications to the wormlike chain model have also been applied to DNA stretching and were reviewed in Ref. 30. A comprehensive introduction to persistence length, contour length, and filament models can be found in Refs. 31 and 32.

B. DNA tether stretching: Materials and methods

The assay geometry arranges a 3500 base pair double stranded DNA (dsDNA) tether between the coverglass surface and a bead. The tether attachment is mediated by a digoxigenin/anti-digoxigenin interaction at the coverglass surface and a biotin/avidin connection to the bead. The construction of the tether geometry is split into production of the dsDNA complexes and final assembly of the tether in the flow cell.

The 3500 base pair dsDNA tether complexes are constructed using a polymerase chain reaction (PCR) technique to amplify a segment of the M13mp18 plasmid (Bayou Biolabs) making multiple copies with appropriate functional ends. PCR is a common biological technique and information on the method can be found in Ref. 33. Amplification is accomplished using Taq polymerase (Invitrogen). A 5′ forward primer functionalized with biotin ([biotin]-5′-AAT CCG CTT TGC TTC TGA CT-3′, Integrated DNA Technologies) and a 5′ reverse primer with digoxigenin ([digoxigenin]-5′-TTG AAA TAC CGA CCG TGT GA-3′, Integrated DNA Technologies) yield a tether with a biotin moiety on one end and a digoxigenin on the other.

Each PCR reaction tube contains 10 μL of 10× PCR buffer (Invitrogen), 3 μL of 50 mM MgCl$_2$ (Invitrogen), 10 μL of 2.5 mM dNTP cocktail (6 μL of 100 mM dATP, 6 μL of 100 mM dCTP, 6 μL of 100 mM dGTP, 6 μL of 100 mM dTTP, Invitrogen), 2 μL of Taq polymerase, and 61 μL of H$_2$O. To this mixture a combination of 10 μL of 5 μg/mL M13mp18 in a TE buffer (1 mM Tris, Sigma, 1 mM EDTA, Acros, pH 7.5) and 2 μL each of the 20 μM forward and reverse primers in TE buffer is added.

The mixture is run in a PCR machine with a primary denaturation cycle at 94 °C for 3 min. Thirty amplification cycles follow, running 1 min at 94 °C for melting, 1 min at 48 °C for annealing, and 7 min of elongation at 72 °C. Each amplification cycle approximately doubles the concentration of the desired 3500 bp segment. A final elongation cycle of 14 min at 72 °C completes the PCR amplification.

The processed tethers are cleaned using a QuiaQuick purification kit (Qiagen). The tether cloning protocol is also available in the supplementary information.[12]

To form DNA tethers between the coverglass surface and a bead, a 1:1 mixture of 20 pM DNA complexes and 1 wt % 1 μm streptavidin coated silica beads (Bangs) is made and incubated for 4 h at 4 °C. A flow cell is created as described previously. A 1:5 dilution of 20 mg/mL anti-digoxigenin (Roche) in PBS (100 mM phosphate buffer, pH 7.4, 0.138M NaCl, 0.0027M KCl, Sigma) is made and further diluted in 1:10 PBT (100 mM phosphate buffer, pH 7.5, 0.1% Tween, Fisher Scientific). The flow cell is loaded with 25 μL of the anti-digoxigenin solution and incubated for at least 40 min at room temperature. To prevent nonspecific attachment, 200 μL of a 1 mg/mL dilution of casein (Sigma) in PBT is loaded into the flow cell, using a vacuum to draw the liquid through the flow chamber. The casein solution is incubated for ~20 min at room temperature. The bead:DNA complexes are pelleted by spinning at 9000 g for 6 min and the supernatant is removed. The bead:DNA complexes are resuspended in PBT and diluted by a factor of 4. Then 25 μL of bead:DNA complexes are loaded into the flow cell using the vacuum and incubated for ~20 min. As a final wash step, 800 μL of a 1 mg/mL dilution of casein in PBT, is drawn through the flow cell using the vacuum. This process produces DNA tethers between the etched glass coverslip and the silica beads. A complimentary description of this process can be found in Ref. 3. PCR production of the DNA tethers can be done far ahead of time, with DNA samples stored frozen at −20 °C. Preparation of the slides must be done immediately prior to use and is best done by an instructor who is familiar with the protocol.

Once loaded on the microscope, visual examination of the slide allows the identification of tethered beads through their restricted Brownian motion. When located, the sample is moved to position the tether in the center of the trap. The height of the bead above the surface is adjusted so that the bead is just touching the surface. This adjustment can be accomplished by finding the point at which the bead begins to defocus when the coverslip is moved closer to the trap, and positioning the bead and trap just above this point. Picomotor based stage movement translates the tether 2500 nm out of the center of the trap, then begins stepping the bead back through the trap in 30 nm increments at an average rate of 100 nm/s. Bead position data are acquired simultaneously with the sweep. As the tether moves through the trap, the bead is captured by the optical trap, creating a situation where the tether is fully stretched, allowed to slacken, and then stretched again. The stretching curve initially obtained reflects the displacement of the bead out of the trap on both sides with a flat, slack region in the center versus the stage position (Fig. 8).

The stage position versus detector voltage data is converted to force versus stage position using calibration parameters (Sec. III). One half of the tether extension is extracted from the data by truncating the curve from the midpoint of the plateau (Fig. 8, label B) to one end of the linear region of
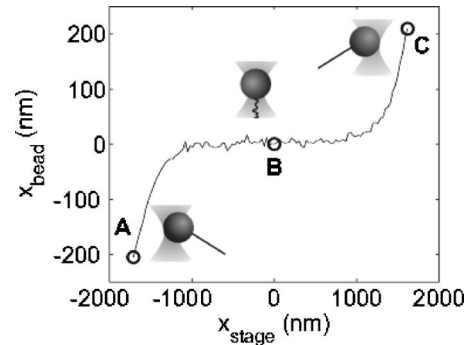

Fig. 8. Bead displacement x_{bead} out of the center of the trap versus stage position x_{stage} of a 3500 bp DNA tether. The cartoons illustrate the relative position of the trap, bead, and tether. The labels A and C indicate the approximate end of the linear portion of stretching curve. Label B is located at the center of the stretching curve. The flat area indicates a slack tether where the DNA is under no tension.

the extension curve (Fig. 8, label A or C). This segment of the curve yields data from a slack tether to the end of the linear region of force applied by the trap. The tether extension is calculated as follows, taking into account the bead radius r and the height h above the surface (see Fig. 9, inset),

$$x = \sqrt{h^2 + (x_{\text{stage}} - x_{\text{bead}})^2} - r, \tag{8}$$

where x is the tether length, x_{stage} is the stage position, and x_{bead} is the displacement of the bead out of the center of the trap. The values for ℓ_p and ℓ_c are extracted by performing a fit of the converted data to the interpolation of the wormlike chain, Eq. (7), using a nonlinear curve fitting algorithm such as nlinfit (Matlab) (see Fig. 9).

Alternatively, students can work backward to determine the position and stiffness calibrations by using the DNA stretching curve as an internal calibration standard. The calibration factors can be extracted by fixing ℓ_p and ℓ_c to calculate a force versus stage position curve and fitting the acquired data by optimizing the stiffness, k, and position calibration, ρ.

C. DNA tether stretching: Experimental results

Accepted persistence lengths for dsDNA fall between 40 and 50 nm, and the contour length for a 3500 base pair strand is expected to be around 1180 nm.[29,30] The wormlike
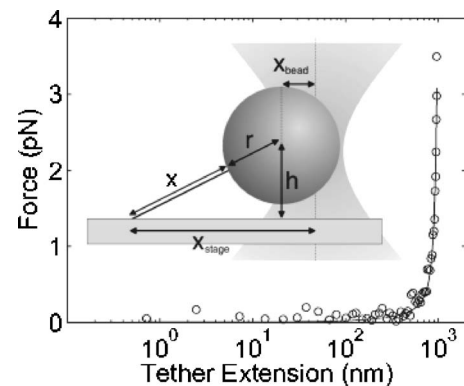

Fig. 9. Force versus extension curve for one of the 3500 bp DNA tethers. The wormlike chain fit gives $\ell_p = 29.9$ nm and $\ell_c = 1077.8$ nm. The inset cartoons show the relevant distances for calculating the tether extension x.
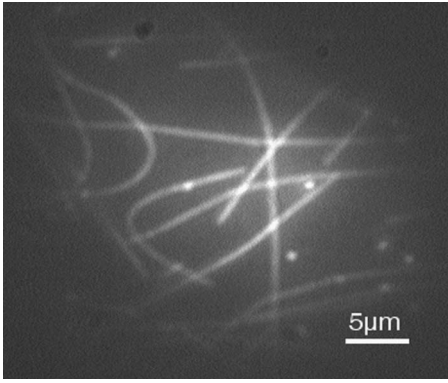
Fig. 10. Rhodamine labeled microtubules excited with the 532 nm laser; the fluorescence emission peak is at 585 nm. The excitation zone is approximately 20 μm in diameter.

chain fit applied to a variety of our data sets produced persistence lengths between 10 and 50 nm with contour lengths from 1000 to 1200 nm. It takes a number of tries and practice to obtain a clean stretching curve. One slide contains many tethered beads to examine and five to ten stretching curves can be obtained in an hour. Improvements in centering the bead over the tether on the coverslip prior to an experiment and more accurately setting the height of the bead above the surface would help to further refine the results. A portion of the error in measuring ℓ_p and ℓ_c is due to the uncertainty of the calibration parameters. The instrument can assay force-extension curves for DNA, giving results close to accepted literature values culminating in an excellent single-molecule laboratory module.

VI. EXPERIMENT: ADDITIONAL MODULES

Further experimental development is encouraged to take advantage of the fluorescence and detection capabilities of the instrument. For example, rhodamine labeled microtubules can be visualized easily with this instrument as the peak excitation occurs at 535 nm and the emission peak is at 585 nm. Preparation of fluorescent microtubules like those in Fig. 10 is given in Ref. 12. These microtubules can be used as a base for a gliding filament assay, bead motility, or kinesin stepping module.[34] The persistence length of microtubules can be used by monitoring their thermal motion or through direct buckling using the optical trap.[32]

The calibration module can be expanded by using solutions of different viscosities and varying the bead diameter to see how these parameters affect trap stiffness and the forces involved. The DNA stretching module can be extended using a higher power laser to demonstrate DNA shearing and unzipping or the opening of hairpins.

With the flexibility of the optics, other basic microscopy modules can be developed. Basic techniques in optical design and measurement can be examined, such as measuring the beam diameter with a razorblade.[35] Advanced students can build and align the trap as part of a long term project; most labs will probably find assembly by students to be a large time commitment and prefer to use prebuilt traps. For courses that emphasize optics, components of this instrument (the lamp, condenser objective, tube lens, and camera) can

form a construction set for students to build a simple microscope. Community contribution of further experiments is highly encouraged on the online resource.[12]

VII. CONCLUSIONS

An inexpensive, fully functional optical trap can be constructed for use as a teaching tool for undergraduate laboratory environments. The integrated position detection, stage movement, and fluorescence provide a solid foundation for many in-depth experiments. Laboratory modules geared toward understanding optical trapping fundamentals, exploring single molecule biophysics, and examining molecular motors have been created. The flexibility of this design promotes further experimental development.

[a])Electronic mail: mjlang@mit.edu
[1] A. Ashkin, "Acceleration and trapping of particles by radiation pressure," Phys. Rev. Lett. **24**(4), 156–159 (1970).
[2] M. J. Lang and S. M. Block, "Resource Letter: LBOT-1: Laser-based optical tweezers," Am. J. Phys. **71**(3), 201–215 (2003).
[3] M. J. Lang, P. M. Fordyce, A. M. Engh, K. C. Neuman, and S. M. Block, "Simultaneous, coincident optical trapping and single-molecule fluorescence," Nat. Methods **1**(2), 133–139 (2004).
[4] K. Visscher, M. J. Schnitzer, and S. M. Block, "Single kinesin molecules studied with a molecular force clamp," Nature (London) **400**, 184–189 (1999).
[5] A. Ishijima, H. Kojima, T. Funatsu, M. Tokunaga, H. Higuchi, H. Tanaka, and T. Yanagida, "Simultaneous observation of individual ATPase and mechanical events by a single myosin molecule during interaction with actin," Cell **92**(2), 161–171 (1998).
[6] C. G. Galbraith and M. P. Sheetz, "Keratocytes pull with similar forces on their dorsal and ventral surfaces," J. Cell Biol. **147**(6), 1313–1324 (1999).
[7] S. P. Smith, S. R. Bhalotra, A. L. Brody, B. L. Brown, E. K. Boyda, and M. Prentiss, "Inexpensive optical tweezers for undergraduate laboratories," Am. J. Phys. **67**(1), 26–35 (1999).
[8] R. Pastel, A. Struthers, R. Ringle, J. Rogers, C. Rohde, and P. Geiser, "Laser trapping of microscopic particles for undergraduate experiments," Am. J. Phys. **68**(11), 993–1001 (2000).
[9] D. N. Moothoo, J. Arlt, R. S. Conroy, F. Akerboom, A. Voit, and K. Dholakia, "Beth's experiment using optical tweezers," Am. J. Phys. **69**(3), 271–276 (2001).
[10] J. Bechhoefer and S. Wilson, "Faster, cheaper, safer optical tweezers for the undergraduate laboratory," Am. J. Phys. **70**(4), 393–400 (2002).
[11] K. C. Neuman, E. H. Chadd, F. G. Liou, K. Bergman, and S. M. Block, "Characterization of photodamage to Escherichia coli in optical traps," Biophys. J. **77**(5), 2856–2863 (1999).
[12] ⟨http://www.openwetware.org/wiki/Optical_Trap⟩
[13] K. Svoboda and S. M. Block, "Biological applications of optical forces," Annu. Rev. Biophys. Biomol. Struct. **23**, 247–285 (1994).
[14] M. P. Sheetz, "Laser tweezers in cell biology," Methods Cell Biol. **55**, 111–112 (1998).
[15] M. J. Lang, C. L. Asbury, J. W. Shaevitz, and S. M. Block, "An auto-

mated two-dimensional optical force clamp for single molecule studies," Biophys. J. **83**(1), 491–501 (2002).

[16] M. W. Allersma, F. Gittes, M. J. deCastro, R. J. Stewart, and C. F. Schmidt, "Two-dimensional tracking of ncd motility by back focal plane interferometry," Biophys. J. **74**(2), 1074–1085 (1998).

[17] K. M. Addas, C. F. Schmidt, and J. X. Tang, "Microrheology of solutions of semiflexible biopolymer filaments using laser tweezers interferometry," Phys. Rev. E **70**, 021503-1–16 (2004).

[18] K. Berg-Sorensen and H. Flyvbjerg, "Power spectrum analysis for optical tweezers," Rev. Sci. Instrum. **75**(3), 594–612 (2004).

[19] K. C. Neuman and S. M. Block, "Optical trapping," Rev. Sci. Instrum. **75**(9), 2787–2809 (2004).

[20] J. T. Finer, R. M. Simmons, and J. A. Spudich, "Single Myosin molecule mechanics: Piconewton forces and nanometer steps," Nature (London) **368**(6467), 113–119 (1994).

[21] B. E. Scharf, K. A. Fahrner, L. Turner, and H. C. Berg, "Control of direction of flagellar rotation in bacterial chemotaxis," Proc. Natl. Acad. Sci. U.S.A. **95**(1), 201–206 (1998).

[22] R. M. Berry and H. C. Berg, "Torque generated by the flagellar motor of Escherichia coli while driven backward," Biophys. J. **76**(1), 580–587 (1999).

[23] H. C. Berg, *Random Walks in Biology* (Princeton U. P., Princeton, NJ, 1993).

[24] Gift of Dr. Karen Fahrner, Harvard University.

[25] K. Barker, *At the Bench: A Laboratory Navigator* (Cold Spring Harbor Laboratory, Woodbury, NY, 1998).

[26] M. Silverman and M. Simon, "Flagellar rotation and the mechanism of bacterial motility," Nature (London) **249**, 73–74 (1974).

[27] M. D. Wang, M. J. Schnitzer, H. Yin, R. Landick, J. Gelles, and S. M. Block, "Force and velocity measured for single molecules of RNA polymerase," Science **282**(5390), 902–907 (1998).

[28] H. Miyata, H. Yoshikawa, H. Hakozaki, N. Suzuki, T. Furuno, A. Ikegami, K. Kinosita, Jr., T. Nishizaka, and S. Ishiwata, "Mechanical measurements of single actomyosin motor force," Biophys. J. **68**(4 Suppl), 286S–289S (1995).

[29] J. F. Marko and E. D. Siggia, "Stretching DNA," Macromolecules **28**(26), 8759–8770 (1995).

[30] M. D. Wang, H. Yin, R. Landick, J. Gelles, and S. M. Block, "Stretching DNA with optical tweezers," Biophys. J. **72**(3), 1335–1346 (1997).

[31] P. Nelson, *Biological Physics: Energy, Information, Life* (W. Freeman, New York, 2004).

[32] D. Boal, *Mechanics of the Cell* (Cambridge U. P., Cambridge, UK, 2002).

[33] F. M. Ausubel, R. Brent, R. E. Kingston, D. D. Moore, J. G. Seidman, J. A. Smith, and K. Struhl, *Short Protocols in Molecular Biology*, 5th ed. (Wiley, New York, 2002).

[34] E. Berliner, H. K. Mahtani, S. Karki, L. F. Chu, J. E. Cronan, Jr., and J. Gelles, "Microtubule movement by a biotinated kinesin bound to streptavidin-coated surface," J. Biol. Chem. **269**(11), 8610–8615 (1994).

[35] J. M. Khosrofian and B. A. Garetz, "Measurement of a Gaussian laser-beam diameter through the direct inversion of knife-edge data," Appl. Opt. **22**(21), 3406–3410 (1983).

THE NATURAL WORLD

"The natural world is much more imaginative than we ever imagined. When the imagination of humans held sway, human beings stood on a flat Earth, positioned on the back of an elephant, which was supported on the back of a turtle, and so on. Instead, the Earth is a spinning ball hurtling around a nearby star and the human population stands on this globe, half of us upside-down relative to the other half. When the human imagination was the guide, the matter of the universe consisted of earth, water, air, and fire. Instead, matter consists of atoms in motion, which in turn are made of electrons, protons, and neutrons, and the proton and deuteron, in turn, consist of quarks and gluons. In addition, the so-called vacuum is pulsating with activity."

John S. Rigden, *Hydrogen: The Essential Element* (Cambridge University Press, Cambridge, Massachusetts, 2005), pp. 169–170.